Chapter 8

Algorithms for the Full Potential Equation

8.1 Introduction

Following the success of the Murman-Cole algorithm applied solve the Transonic Small Disturbance equation, the rush was on to extend this procedure to the Full Potential equation (see Section 1.5), capable of describing the flow about blunt nosed airfoils and wings.. Straight forward application of the algorithm to the Full Potential equation failed. Jameson diagnosed the numerical stability difficulty and provided the remedy, as discussed below.

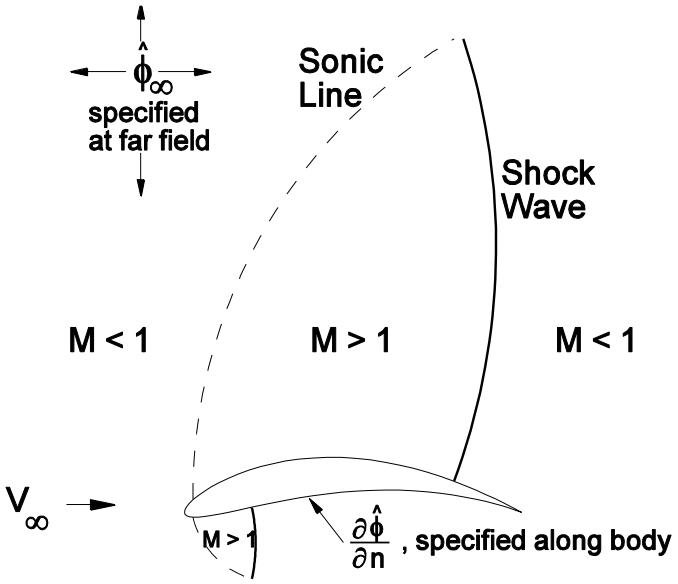

Figure 8.1 Transonic flow past an airfoil.

8.2 Jameson's Rotated Difference Method (1973)

The Full Potential Equation in two dimensions is

$$(a^2-\phi_x^2)\phi_{xx}-2\phi_x\phi_y\phi_{xy}+(a^2-\phi_y^2)\phi_{yy}=0$$

with velocities given by $u=\phi_x$ and $v=\phi_y$. Neither velocity component is necessarily small with respect to free stream velocity $\vec{V}_\infty = u_\infty \vec{i}_x + v_\infty \vec{i}_y$.

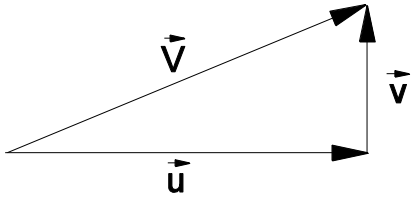

Figure 8.2 Velocity vector.

The major difficulty in applying the Murman-Cole type dependent difference scheme directly to the full potential equation is in determining when and when not to change from central to backward difference approximations. For example, if the flow is supersonic, $V > a = \sqrt{\gamma \frac{p}{\rho}}$, backward difference approximations are required for at least some of the derivative approximations. However, even if $V > a$, each velocity component could still be subsonic, $u < a$ and $v < a$, which suggests central difference approximations for both ϕ_{xx} and ϕ_{yy}. Jameson removed the ambiguity in the choice of difference approximations by locally rotating the coordinate system into alignment with the flow direction. Choices made in the rotated coordinate system were then used to determine the difference approximations in the $x-y$ coordinate system or in the transformed computational space.

Jameson's rotated coordinates are shown to the right. The coordinate s is rotated into alignment with the local velocity vector and n is orthogonal to s.

$$\frac{\partial x}{\partial s} = \cos\theta = \frac{u}{|\vec{V}|}, \quad \frac{\partial x}{\partial n} = -\sin\theta = \frac{-v}{|\vec{V}|},$$

$$\frac{\partial y}{\partial s} = \sin\theta = \frac{v}{|\vec{V}|}, \quad \frac{\partial y}{\partial n} = \cos\theta = \frac{u}{|\vec{V}|}$$

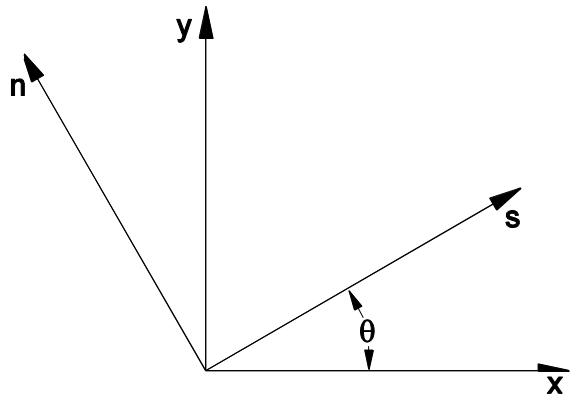

Figure 8.3 Rotated coordinates.

The Full Potential equation in transformed coordinates is

$$(a^2 - V^2)\phi_{ss} + a^2\phi_{nn} = 0$$

The Murman-Cole scheme can now be applied directly to the transformed equation as follows

(i) ϕ_{nn} term is central differenced.

(ii) If $V^2 < a^2$, the ϕ_{ss} term is also central differenced.

(iii) If $V^2 > a^2$, the ϕ_{ss} term is backward differenced.

In terms of the original coordinate system

$$\phi_{ss} = (u^2\phi_{xx} + 2uv\phi_{xy} + v^2\phi_{yy})/V^2$$
$$\phi_{nn} = (v^2\phi_{xx} - 2uv\phi_{xy} + u^2\phi_{yy})/V^2$$

Jameson's difference approximation to the Full Potential equation in the $x-y$ coordinate system, is as follows.

(i) The terms ϕ_{xx} ϕ_{xy} and ϕ_{yy} appearing in ϕ_{nn} are central differenced

$$\phi_{xx} \simeq \frac{D_{xx}}{\Delta x^2}\cdot\phi_{i,j} = \frac{\phi_{i+1,j} - 2\phi_{i,j} + \phi_{i-1,j}}{\Delta x^2}$$

$$\phi_{xy} \simeq \frac{\phi_{i+1,j+1} - \phi_{i-1,j+1} - \phi_{i+1,j-1} + \phi_{i-1,j-1}}{2\Delta x 2\Delta y}$$

$$\phi_{yy} \simeq \frac{D_{yy}}{\Delta y^2}\cdot\phi_{i,j} = \frac{\phi_{i,j+1} - 2\phi_{i,j} + \phi_{i,j-1}}{\Delta y^2}$$

(ii) If $V^2 < a^2$, the subsonic case, the terms ϕ_{xx} ϕ_{xy} and ϕ_{yy} appearing in ϕ_{ss} are also central differenced as above.

(iii)} If $V^2 > a^2$, the supersonic case, the terms ϕ_{xx} ϕ_{xy} and ϕ_{yy} appearing in ϕ_{ss} are backward differenced in the appropriate stencil quadrant about mesh point i, j, as illustrated below for both u *and* $v \geq 0$.

$$\phi_{xx} \simeq \frac{D_{xx}}{\Delta x^2}\cdot\phi_{i-1,j} = \frac{\phi_{i,j} - 2\phi_{i-1,j} + \phi_{i-2,j}}{\Delta x^2}$$

$$\phi_{xy} \simeq \frac{\phi_{i,j} - \phi_{i-1,j} - \phi_{i,j-1} + \phi_{i-1,j-1}}{\Delta x \Delta y}$$

$$\phi_{yy} \simeq \frac{D_{yy}}{\Delta y^2}\cdot\phi_{i,j-1} = \frac{\phi_{i,j} - 2\phi_{i,j-1} + \phi_{i,j-2}}{\Delta y^2}$$

The difference in the supersonic and subsonic approximations for the ϕ_{ss} term is shown below.

$$\left\{\begin{matrix}Supersonic\\ Differencing\end{matrix}\right\}\cdot\phi_{ss} = \left\{\begin{matrix}Subsonic\\ Differencing\end{matrix}\right\}\cdot\phi_{ss} - (a^2 - V^2)\Delta s\phi_{sss} + \cdots$$

$$but \quad -(a^2 - V^2)\Delta s\phi_{sss} = (V^2 - a^2)\left(\Delta x u^2 \frac{\partial^2 u}{\partial x^2} + \cdots\right)$$

The term above represents a viscous-like dissipative term that is effectively added to the central difference approximation through the change to a backward difference approximation in supersonic regions. This change stabilizes the calculation.

8.3 Holst's Method for the Full Potential Equation in Conservation Law Form (1979)

Following Jameson's breakthrough, enabling the application of the Murman-Cole strategy for the Full Potential Equation in non-conservation form, Holst extended the concept to the equation in conservation form. This is an important extension, more than just satisfying the conservation of mass within the computed flow field, because it enables the equations to be easily expressed in arbitrary curvilinear coordinate systems, particularly computational coordinates for body fitted meshes, using the concepts discussed in Chapter 7. We start with a description in Cartesian coordinates

The Euler continuity equation (see Section 1.4) expressed in terms of the full potential ϕ in Cartesian coordinates in two dimensions is

$$\frac{\partial(\rho\phi_x)}{\partial x}+\frac{\partial(\rho\phi_y)}{\partial y}=0, \quad and$$

$$\rho=\rho_\infty\left[1-\frac{\gamma-1}{2}M_\infty^2\left(\frac{\phi_x^2+\phi_y^2}{V_\infty^2}-1\right)\right]^{\frac{1}{\gamma-1}}$$

If we again use Jameson's rotated coordinates, given in Section 8.2, to express the Full Potential equation at a point in space, we obtain.

$$\frac{\partial(\rho\phi_s)}{\partial s}+\frac{\partial(\rho\phi_n)}{\partial n}=0 \qquad (8.2.1)$$

$$\rho=\rho_\infty\left[1-\frac{\gamma-1}{2}M_\infty^2\left(\frac{\phi_s^2+\phi_n^2}{V_\infty^2}-1\right)\right]^{\frac{1}{\gamma-1}} \text{ with } V=u'=\frac{\partial\phi}{\partial s} \text{ and } v'=\frac{\partial\phi}{\partial n}=0$$

Because the density ρ is always positive Equation (8.2.1) appears to be always elliptic, but this is not true as we will now show.

The pressure can be expressed as $p=p_\infty\left[1-\frac{\gamma-1}{2}M_\infty^2\left(\frac{\phi_s^2+\phi_n^2}{V_\infty^2}-1\right)\right]^{\frac{\gamma}{\gamma-1}}$. The square of the speed of sound a^2 can be expressed as

$$a^2=\gamma\frac{p}{\rho}=a_\infty^2\left[1-\frac{\gamma-1}{2}M_\infty^2\left(\frac{\phi_s^2+\phi_n^2}{V_\infty^2}-1\right)\right]=a_\infty^2\left[1-\frac{\gamma-1}{2}M_\infty^2\left(\frac{V^2}{V_\infty^2}-1\right)\right] \qquad (8.2.2)$$

For analysis, we can write the rotated Full Potential equation in non-conservation form as

$$\rho\frac{\partial\phi_s}{\partial s}+u'\frac{\partial\rho}{\partial s}+\rho\frac{\partial\phi_n}{\partial n}+v'\frac{\partial\rho}{\partial n}=0$$

$$\text{but}\quad u'\frac{\partial\rho}{\partial s}=u'\frac{\partial\rho}{\partial u'}\frac{\partial u'}{\partial s}=-\rho\frac{M_\infty^2\dfrac{u'^2}{V_\infty^2}}{1-\dfrac{\gamma-1}{2}M_\infty^2\left(\dfrac{V^2}{V_\infty^2}-1\right)}\frac{\partial u'}{\partial s}=-\rho\frac{V^2}{a^2}\frac{\partial\phi_s}{\partial s}$$

The above rotated Full Potential equation then becomes

$$\rho\left(1-\frac{V^2}{a^2}\right)\frac{\partial\phi_s}{\partial s}+\rho\frac{\partial\phi_n}{\partial n}=0$$

It is now clear from the above that this equation becomes hyperbolic whenever the flow becomes supersonic, just as before for the Full Potential equation studied in Section 8.2. We also observe that the mechanism that causes the equation to change type occurs through the variation of density. Holst's algorithm uses the variation in density to determine when to change the difference equation in supersonic regions to maintain numerical stability. The algorithm applied to Equation (8.2.1) is given below.

$$\left\{\tilde\rho_{i+1/2,j}\frac{\phi_{i+1,j}-\phi_{i,j}}{\Delta s}-\tilde\rho_{i-1/2,j}\frac{\phi_{i,j}-\phi_{i-1,j}}{\Delta s}\right\}\frac{1}{\Delta s}+\left\{\rho_{i,j+1/2}\frac{\phi_{i,j+1}-\phi_{i,j}}{\Delta n}-\rho_{i,j-1/2}\frac{\phi_{i,j}-\phi_{i,j-1}}{\Delta n}\right\}\frac{1}{\Delta n}=0$$

The switching seen earlier for the Murman-Cole and Jameson methods for the potential equations also appears in the above Holst difference equations through the evaluation of the densities marked with "tildes" in the stream-wise derivative approximations. We first define the Mach number switch function, illustrated at surface $i+1/2, j$.

$$\nu_{i+1/2,j}=\max\left\{0,\tilde M^2_{i+1/2,j}-1\right\},\ \text{with}\ \tilde M^2_{i+1/2,j}=\begin{cases}M^2_{i,j} & \text{if}\ \ u'_{i+1/2,j}\ge 0\\ M^2_{i+1,j} & \text{if}\ \ u'_{i+1/2,j}<0\end{cases}$$

The Mach numbers defined above at whole integer index values use centered differences to define the velocities as derivatives of ϕ, i.e. $u'_{i,j}=\dfrac{\phi_{i+1,j}-\phi_{i-1,j}}{2\Delta s}$, and the velocities shown above with half integer values are centered at the flux surfaces indicated, i.e. $u'_{i+1/2,j}=\dfrac{\phi_{i+1,j}-\phi_{i,j}}{\Delta s}$, etc.

The velocity dependent or "retarded" densities are defined as follows.

$$\tilde{\rho}_{i+1/2,j} = (1-\nu_{i+1/2,j})\rho_{i+1/2,j} + \begin{cases} \nu_{i+1/2,j}\rho_{i-1/2,j}, & if \;\; u'_{i,j} \geq 0 \\ or & \\ \nu_{i+1/2,j}\rho_{i+3/2,j}, & if \;\; u'_{i,j} \leq 0 \end{cases}$$

The effect of the retardation of density for regions of supersonic flow can be shown to be

$$\begin{Bmatrix} Supersonic \\ Differencing \end{Bmatrix} \cdot \frac{\partial \rho u'}{\partial s} = \begin{Bmatrix} Subsonic \\ Differencing \end{Bmatrix} \cdot \frac{\partial \rho u'}{\partial s} - \frac{\partial (\nu \Delta s \frac{\partial \rho}{\partial s} u')}{\partial s}$$

$$= \begin{Bmatrix} Subsonic \\ Differencing \end{Bmatrix} \cdot \frac{\partial \rho u'}{\partial s} - \frac{\partial (\nu \frac{u'^2}{a^2} \Delta s \frac{\partial u'}{\partial s})}{\partial s}$$

The latter term is equivalent to the addition of a viscous term of viscosity equal to $\nu \frac{u'^2}{a^2} \Delta s$. It also lowers the order of accuracy to first order in supersonic regions. The above description of Holst's method has been simplified to concentrate on the main ideas. Fuller expressions of this method, with both higher order accuracy approximations and enhanced stability options in supersonic regions, can be found in the literature. We proceed with the basic algorithm applied to the Full Potential Equation in arbitrary coordinates.

8.3.1 Full Potential Equation in Arbitrary Coordinates

The Full Potential Equation in conservation law form can be rewritten as follows

$$\frac{\partial F}{\partial x} + \frac{\partial G}{\partial y} = 0 \;\; \text{where} \;\; F = \rho \phi_x \;\; \text{and} \;\; G = \rho \phi_y$$

We transform this equation for solution in the computational ξ and η plane. See Section 7.3, ***"Conservation laws map into conservation laws".*** The coordinates ξ and η are not necessarily the same as s and n used in the section above, but ξ will be considered to be essentially in the stream-wise direction when and if the flow becomes supersonic. The body fitted computational meshes used below to illustrate the application of the Holst Algorithm will have this property.

$$\frac{\partial F'}{\partial \xi} + \frac{\partial G'}{\partial \eta} = 0 \;\; \text{with} \;\; F' = \rho \left\{ \phi_x \frac{\partial y}{\partial \eta} - \phi_y \frac{\partial x}{\partial \eta} \right\} \;\; \text{and} \;\; G' = \rho \left\{ -\phi_x \frac{\partial y}{\partial \xi} + \phi_y \frac{\partial x}{\partial \xi} \right\}$$

$$\text{with} \quad \begin{bmatrix} \frac{\partial \phi}{\partial x} \\ \frac{\partial \phi}{\partial y} \end{bmatrix} = \frac{1}{d_{xy}} \begin{bmatrix} \frac{\partial y}{\partial \eta} & -\frac{\partial y}{\partial \xi} \\ -\frac{\partial x}{\partial \eta} & \frac{\partial x}{\partial \xi} \end{bmatrix} \begin{bmatrix} \frac{\partial \phi}{\partial \xi} \\ \frac{\partial \phi}{\partial \eta} \end{bmatrix} \quad \textit{and} \quad d_{xy} = \frac{\partial x}{\partial \xi}\frac{\partial y}{\partial \eta} - \frac{\partial x}{\partial \eta}\frac{\partial y}{\partial \xi}$$

By substitution

$$\begin{bmatrix} F' \\ G' \end{bmatrix} = \frac{\rho}{d_{xy}} \begin{bmatrix} \frac{\partial y}{\partial \eta}\frac{\partial y}{\partial \eta} + \frac{\partial x}{\partial \eta}\frac{\partial x}{\partial \eta} & -\frac{\partial x}{\partial \xi}\frac{\partial x}{\partial \eta} - \frac{\partial y}{\partial \xi}\frac{\partial y}{\partial \eta} \\ -\frac{\partial x}{\partial \xi}\frac{\partial x}{\partial \eta} - \frac{\partial y}{\partial \xi}\frac{\partial y}{\partial \eta} & \frac{\partial x}{\partial \xi}\frac{\partial x}{\partial \xi} + \frac{\partial y}{\partial \xi}\frac{\partial y}{\partial \xi} \end{bmatrix} \begin{bmatrix} \frac{\partial \phi}{\partial \xi} \\ \frac{\partial \phi}{\partial \eta} \end{bmatrix} = \begin{bmatrix} T_{11} & T_{12} \\ T_{21} & T_{22} \end{bmatrix} \begin{bmatrix} \frac{\partial \phi}{\partial \xi} \\ \frac{\partial \phi}{\partial \eta} \end{bmatrix}$$

We can also define the primed velocity coordinates u' and v', which represent the velocity components normal to constant coordinate lines ξ and η, respectively.

$$\begin{bmatrix} F' \\ G' \end{bmatrix} = \begin{bmatrix} \rho u' \\ \rho v' \end{bmatrix} = \begin{bmatrix} T_{11} & T_{12} \\ T_{21} & T_{22} \end{bmatrix} \begin{bmatrix} \frac{\partial \phi}{\partial \xi} \\ \frac{\partial \phi}{\partial \eta} \end{bmatrix}$$

Using the **generic equation** form from Section 7.7.3 for the steady Full Potential equation

$$\frac{F'_{i+1/2,j} - F'_{i-1/2,j}}{\Delta \xi} + \frac{G'_{i,j+1/2} - G'_{i,j-1/2}}{\Delta \eta} = 0$$

8.3.2 Solution Approach

8.3.2.1 Evaluation of the Derivative Terms

Both F' and G' contain derivatives of ϕ as well as metric term derivatives. The derivative terms need to be evaluated centered about the surface at which the flux crosses, as discussed in Section 7.8. The metric terms, including those within $d_{xy_{i+1/2,j}}$, are evaluated in Section 7.8.4. The derivatives of ϕ at surface $\xi = i + 1/2$ are evaluated as follows.

$$\left.\frac{\partial \phi}{\partial \xi}\right|_{i+1/2,j} \simeq \frac{D_+ \cdot \phi_{i,j}}{\Delta \xi} = \frac{\phi_{i+1,j} - \phi_{i,j}}{\Delta \xi}$$

$$\left.\frac{\partial \phi}{\partial \eta}\right|_{i+1/2,j} \simeq \frac{D_0 \cdot (\phi_{i,j} + \phi_{i+1,j})/2}{\Delta \eta}$$

$$= \frac{\phi_{i,j+1} + \phi_{i+1,j+1} - \phi_{i,j-1} - \phi_{i+1,j-1}}{4\Delta \eta}$$

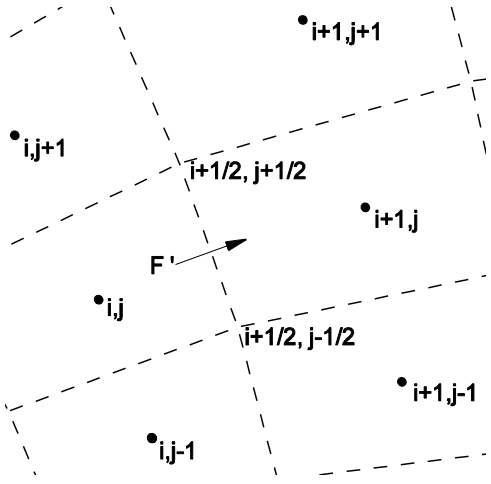

Similarly, the derivatives of ϕ at surface $\eta = j+1/2$ are evaluated as follows.

$$\left.\frac{\partial\phi}{\partial\xi}\right|_{i,j+1/2} \simeq \frac{D_0\cdot(\phi_{i,j}+\phi_{i,j+1})/2}{\Delta\xi}$$

$$= \frac{\phi_{i+1,j}+\phi_{i+1,j+1}-\phi_{i-1,j}-\phi_{i-1,j+1}}{4\Delta\xi}$$

$$\left.\frac{\partial\phi}{\partial\eta}\right|_{i,j+1/2} \simeq \frac{D_+\cdot\phi_{i,j}}{\Delta\eta} = \frac{\phi_{i,j+1}-\phi_{i,j}}{\Delta\eta}$$

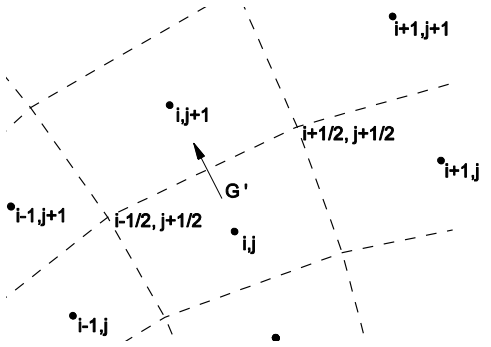

8.3.2.2 The Holst Switch Function

The switch function, $\nu = \max\{0, M^2-1\}$, is used to determine $\tilde{\rho}$, where $V^2 = u^2+v^2$, the sound speed $a = \sqrt{\gamma p/\rho}$,

$$\rho = \rho_\infty\left[1-\frac{\gamma-1}{2}M_\infty^2\left(\frac{u^2+v^2}{V_\infty^2}-1\right)\right]^{\frac{1}{\gamma-1}},$$

$$p = p_\infty\left[1-\frac{\gamma-1}{2}M_\infty^2\left(\frac{u^2+v^2}{V_\infty^2}-1\right)\right]^{\frac{\gamma}{\gamma-1}},$$

$$u = \phi_x = \frac{1}{d_{xy}}\left(\frac{\partial y}{\partial\eta}\phi_\xi - \frac{\partial x}{\partial\eta}\phi_\eta\right) \text{ and } v = \phi_y = \frac{1}{d_{xy}}\left(-\frac{\partial y}{\partial\xi}\phi_\xi + \frac{\partial x}{\partial\xi}\phi_\eta\right).$$

The Mach number switch function at surface $i+1/2, j$.

$$\nu_{i+1/2,j} = \max\{0, \tilde{M}^2_{i+1/2,j}-1\}, \text{ with } \tilde{M}^2_{i+1/2,j} = \begin{cases} M^2_{i,j} & \text{if } u'_{i+1/2,j} \geq 0 \\ M^2_{i+1,j} & \text{if } u'_{i+1/2,j} < 0 \end{cases}$$

The velocity dependent or "retarded" densities used in the flux terms of form $F' = \rho\left\{\phi_x\frac{\partial y}{\partial\eta} - \phi_y\frac{\partial x}{\partial\eta}\right\}$ are defined as follows.

$$\tilde{\rho}_{i+1/2,j} = (1-\nu_{i,j})\rho_{i+1/2,j} + \begin{cases} \nu_{i,j}\rho_{i-1/2,j}, & \text{if } \phi_{\xi_{i,j}} \geq 0 \\ or & \\ \nu_{i,j}\rho_{i+3/2,j}, & \text{if } \phi_{\xi_{i,j}} \leq 0 \end{cases}$$

8.3.3 ADI Algorithm

We solve the generic difference equation of Section 8.3.1 by the ADI (Alternating Direction Implicit) Method (see Section 5.3) using also the "delta", $\delta\phi$, form of the algorithm (Section 6.5).

Step (1) sweep direction i and line direction j

The scalar tridiagonal equation to be solved in the ADI Method step (1) is

$$b_j^{(1)}\delta\phi_{i,j+1}^{(1)} + a_j^{(1)}\delta\phi_{i,j}^{(1)} + c_j^{(1)}\delta\phi_{i,j-1}^{(1)} = R_{i,j} = \frac{F'^n_{i+1/2,j} - F'^n_{i-1/2,j}}{\Delta\xi} + \frac{G'^n_{i,j+1/2} - G'^n_{i,j-1/2}}{\Delta\eta}$$

$$\text{with } a_j^{(1)} = a_0 + T^n_{11_{i+1/2,j}} + T^n_{11_{i-1/2},j} + T^n_{22_{i,j+1/2}} + T^n_{22_{i,j-1/2}}$$

$$b_j^{(1)} = -T^n_{22_{i,j+1/2}} - \frac{1}{4}(T^n_{12_{i+1/2,j}} - T^n_{12_{i-1/2,j}})$$

$$c_j^{(1)} = -T^n_{22_{i,j-1/2}} + \frac{1}{4}(T^n_{12_{i+1/2,j}} - T^n_{12_{i-1/2,j}})$$

$$\text{and solution update } \phi_{i,j}^{(1)} = \phi_{i,j}^n + \delta\phi_{i,j}^{(1)} \text{ for all } i, j$$

A constant a_0 has been added to the main diagonal term to improve convergence and stability in supersonic regions. A value of $a_0 = 1$ has been used in the all the calculated results to appear in this chapter.

The boundary condition at the body surface is given by

$$v'_{body} = \left.\frac{\partial\phi}{\partial n}\right|_{body} = 0, \quad and \quad \left.\frac{\partial\delta\phi}{\partial n}\right|_{body} = 0$$

$$\text{But} \quad v' = \frac{1}{\rho}\left(T_{21}\frac{\partial\phi}{\partial\xi} + T_{22}\frac{\partial\phi}{\partial\eta}\right),$$

$$\text{hence } \left.\frac{\partial\phi}{\partial\eta}\right|_{body} = -\frac{T_{21}}{T_{22}}\left.\frac{\partial\phi}{\partial\xi}\right|_{body} \text{ and } \left.\frac{\partial\delta\phi}{\partial\eta}\right|_{body} = -\left(\frac{\partial\phi}{\partial\eta} + \frac{T_{21}}{T_{22}}\frac{\partial\phi}{\partial\xi}\right)\Bigg|_{body}$$

Thus, $\phi_{i,1} = \phi_{i,2} + \Delta\eta\left.\frac{T_{21}}{T_{22}}\frac{\partial\phi}{\partial\xi}\right|^n_{body}$ and $\delta\phi_{i,1} = \delta\phi_{i,2} + \Delta\eta\left(\frac{\partial\phi}{\partial\eta} + \frac{T_{21}}{T_{22}}\frac{\partial\phi}{\partial\xi}\right)\Bigg|^n_{body} = R^n_{i,1}$. Note that if the boundary condition on $\phi_{i,1}$ is set, then $R^n_{i,1} = 0$. At the far field boundary $\phi_{i,J}$ is fixed from the initial condition and $\delta\phi_{i,J} = 0$.

Step (2) sweep direction j and line direction i

The scalar tridiagonal equation to be solved in the ADI Method step (2) is

$$b_j^{(2)}\delta\phi_{i,j+1}^{n+1} + a_j^{(2)}\delta\phi_{i,j}^{n+1} + c_j^{(2)}\delta\phi_{i,j-1}^{n+1} = R_{i,j}^{(1)} = \frac{F'^{(1)}_{i+1/2,j} - F'^{(1)}_{i-1/2,j}}{\Delta\xi} + \frac{G'^{(1)}_{i,j+1/2} - G'^{(1)}_{i,j-1/2}}{\Delta\eta}$$

$$\text{with } a_i^{(2)} = a_0 + T11^{(1)}_{i+1/2,j} + T11^{(1)}_{i-1/2,j} + T22^{(1)}_{i,j+1/2} + T22^{(1)}_{i,j-1/2}$$

$$b_i^{(2)} = -T11^{(1)}_{i+1/2,j} - \frac{1}{4}(T21^{(1)}_{i,j+1/2} - T21^{(1)}_{i,j-1/2})$$

$$c_i^{(2)} = -T11^{(1)}_{i-1/2,j} + \frac{1}{4}(T21^{(1)}_{i,j+1/2} - T21^{(1)}_{i,j-1/2})$$

$$\text{and solution update } \phi_{i,j}^{n+1} = \phi_{i,j}^{(1)} + \delta\phi_{i,j}^{n+1} \text{ for all } i, j$$

In addition to the same boundary conditions given previously, the boundary conditions at $i = 1$ and $i = I$ can be of two types in general.

Type (1) Boundaries at $i = 1$ and $i = I$ are in the far field.

$\phi_{1,j}$ and $\phi_{I,j}$ are fixed from the initial condition

and $\delta\phi_{1,j} = \delta\phi_{I,j} = 0$.

Type (2) The mesh wraps around the body and the boundary conditions at $i = 1$ and $i = I$ are periodic.

$$\phi_{I,j} = \phi_{2,j} \text{ and } \phi_{1,j} = \phi_{I-1,j}$$

$$\delta\phi_{I,j} = \delta\phi_{2,j} \text{ and } \delta\phi_{1,j} = \delta\phi_{I-1,j}$$

The solution of Type (2) periodic matrix equations is discussed below.

The matrix inversion procedure required for ADI Step (1) is similar to that discussed in Section 5.3.2, but with different boundary conditions. The matrix to be solved is shown below.

$$\begin{bmatrix} 1 & 0 & 0 & 0 & 0 & 0 & 0 \\ b_{J-1} & a_{J-1} & c_{J-1} & 0 & 0 & 0 & 0 \\ 0 & \ddots & \ddots & \ddots & 0 & 0 & 0 \\ 0 & 0 & b_j & a_j & c_j & 0 & 0 \\ 0 & 0 & 0 & \ddots & \ddots & \ddots & 0 \\ 0 & 0 & 0 & 0 & b_2 & a_2 & c_2 \\ 0 & 0 & 0 & 0 & 0 & -1 & 1 \end{bmatrix} \begin{bmatrix} \delta\phi_{i,J}^{(1)} \\ \delta\phi_{i,J-1}^{(1)} \\ \vdots \\ \delta\phi_{i,j}^{(1)} \\ \vdots \\ \delta\phi_{i,2}^{(1)} \\ \delta\phi_{i,1}^{(1)} \end{bmatrix} = \begin{bmatrix} 0 \\ R_{i,J-1}^n \\ \vdots \\ R_{i,j}^n \\ \vdots \\ R_{i,2}^n \\ R_{i,1}^n \end{bmatrix}$$

For Type (1) boundary conditions the matrix equation to be solved for ADI Step (2) is

$$\begin{bmatrix} 1 & 0 & 0 & 0 & 0 & 0 & 0 \\ b_{I-1} & a_{I-1} & c_{I-1} & 0 & 0 & 0 & 0 \\ 0 & \ddots & \ddots & \ddots & 0 & 0 & 0 \\ 0 & 0 & b_i & a_i & c_i & 0 & 0 \\ 0 & 0 & 0 & \ddots & \ddots & \ddots & 0 \\ 0 & 0 & 0 & 0 & b_2 & a_2 & c_2 \\ 0 & 0 & 0 & 0 & 0 & 0 & 1 \end{bmatrix} \begin{bmatrix} \delta\phi_{I,j}^{n+1} \\ \vdots \\ \vdots \\ \delta\phi_{i,j}^{n+1} \\ \vdots \\ \vdots \\ \delta\phi_{1,j}^{n+1} \end{bmatrix} = \begin{bmatrix} 0 \\ R_{I-1,j}^{(1)} \\ \vdots \\ R_{i,j}^{(1)} \\ \vdots \\ R_{2,j}^{(1)} \\ 0 \end{bmatrix}$$

This matrix equation is also solved similarly to that for ADI Step (1).

For Type (2) boundary conditions, using the periodicity of both the mesh and solution, the matrix equation to be solved is

$$\begin{bmatrix} a_{I-1} & c_{I-1} & 0 & 0 & 0 & 0 & b_{I-1} \\ b_{I-2} & a_{I-2} & c_{I-2} & 0 & 0 & 0 & 0 \\ 0 & \ddots & \ddots & \ddots & 0 & 0 & 0 \\ 0 & 0 & b_i & a_i & c_i & 0 & 0 \\ 0 & 0 & 0 & \ddots & \ddots & \ddots & 0 \\ 0 & 0 & 0 & 0 & b_3 & a_3 & c_3 \\ c_2 & 0 & 0 & 0 & 0 & b_2 & a_2 \end{bmatrix} \begin{bmatrix} \delta\phi_{I-1,j}^{n+1} \\ \vdots \\ \vdots \\ \delta\phi_{i,j}^{n+1} \\ \vdots \\ \vdots \\ \delta\phi_{2,j}^{n+1} \end{bmatrix} = \begin{bmatrix} R_{I,j}^{(1)} \\ \vdots \\ \vdots \\ R_{i,j}^{(1)} \\ \vdots \\ \vdots \\ R_{2,j}^{(1)} \end{bmatrix}$$

The solution of this periodic matrix equation is significantly different than that given in Sections 5.2.2 and 5.3.2 and is discussed in the following section.

8.3.3.1 Periodic Matrix Solution

The periodic matrix of the last section can be factored into upper and lower triangular matrices as shown below.

$$\begin{bmatrix} \alpha_{I-1} & 0 & 0 & 0 & 0 & 0 & 0 \\ b_{I-2} & \alpha_{I-2} & 0 & 0 & 0 & 0 & 0 \\ 0 & \ddots & \ddots & 0 & 0 & 0 & \vdots \\ 0 & 0 & b_i & \alpha_i & 0 & 0 & 0 \\ 0 & 0 & 0 & \ddots & \ddots & 0 & \vdots \\ 0 & 0 & 0 & 0 & b_3 & \alpha_3 & 0 \\ e_{I-1} & e_{I-2} & \cdots & e_i & e_4 & b_2' & \alpha_2 \end{bmatrix} \begin{bmatrix} 1 & \gamma_{I-1} & 0 & 0 & 0 & 0 & d_{I-1} \\ 0 & 1 & \gamma_{I-2} & 0 & 0 & 0 & d_{i-2} \\ 0 & 0 & \ddots & \ddots & 0 & 0 & \vdots \\ 0 & 0 & 0 & 1 & \gamma_i & 0 & d_i \\ 0 & 0 & 0 & 0 & \ddots & \ddots & \vdots \\ 0 & 0 & 0 & 0 & 0 & 1 & \gamma_3' \\ 0 & 0 & 0 & 0 & 0 & 0 & 1 \end{bmatrix} \begin{bmatrix} \delta\phi_{I-1,j}^{n+1} \\ \vdots \\ \vdots \\ \delta\phi_{i,j}^{n+1} \\ \vdots \\ \vdots \\ \delta\phi_{2,j}^{n+1} \end{bmatrix} = \begin{bmatrix} R_{I-1,j}^{(1)} \\ \vdots \\ \vdots \\ R_{i,j}^{(1)} \\ \vdots \\ \vdots \\ R_{2,j}^{(1)} \end{bmatrix}$$

where $\alpha_{I-1} = a_{I-1}$, $\gamma_{I-1} = \dfrac{c_{I-1}}{\alpha_{I-1}}$, $d_{I-1} = \dfrac{b_{I-1}}{\alpha_{I-1}}$,

$$\text{for } i = I-2, \cdots, 3, \quad \alpha_i = a_i - b_i \gamma_{i+1}, \quad \gamma_i = \frac{c_i}{\alpha_i} \quad \text{and} \quad d_i = -\frac{b_i d_{i+1}}{\alpha_i},$$

$$\text{and finally} \quad e_{I-1} = c_2 \quad \text{and} \quad e_i = -e_{i+1}\gamma_{i+1}, \quad \text{for } i = I-2, \cdots, 3,$$

$$b_2' = b_2 + e_3, \quad \gamma_3' = \gamma_3 + d_3 \quad \text{and} \quad \alpha_2 = a_2 - b_2'\gamma_3' - \sum_{i=4}^{I-1} e_i d_i$$

The solution of the above $L \cdot U$ decomposed matrix equation is obtained by a forward elimination down through the L matrix followed by and a backward substitution up through the U matrix.

The forward elimination solves the equation $L\left\{\delta\phi'_{i,j}\right\} = \left\{R^{(1)}_{i,j}\right\}$ as follows

$$\delta\phi'_{I-1} = \frac{R^{(1)}_{I-1,j}}{\alpha_{I-1}} \text{ and then } \delta\phi'_{i,j} = \frac{R^{(1)}_{i,j} - b_i \delta\phi'_{i+1,j}}{\alpha_i}, \text{ for } i = I-2, \cdots, 4, 3.$$

$$\delta\phi'_{2,j} = \frac{R^{(1)}_{2,j} - b_2'\delta\phi'_{3,j} - \sum_{i=4}^{I-1} e_i \delta\phi'_{i,j}}{\alpha_2}$$

The backward substitution solves the equation $U\left\{\delta\phi^{n+1}_{i,j}\right\} = \left\{\delta\phi'_{i,j}\right\}$ as follows

$$\delta\phi^{n+1}_{2,j} = \delta\phi'_{2,j}, \ \delta\phi^{n+1}_{3,j} = \delta\phi'_{3,j} - \gamma_3'\delta\phi^{n+1}_{2,j} \text{ and then}$$

$$\delta\phi^{n+1}_{i,j} = \delta\phi'_{i,j} - \gamma_i \delta\phi^{n+1}_{i-1,j} - d_i \delta\phi^{n+1}_{2,j}, \text{ for } i = 4, \cdots, \mathrm{I}-2, \mathrm{I}-1.$$

8.4 Applications

All of the following applications use the Holst method to solve the Full Potential equation in conservation law form.

8.4.1 Applications 1 : Flow Past a Circular Arc Airfoil

Exercise: Solve for Case (1) subsonic flow at $M_\infty = 0.735$ and Case (2) transonic flow at $M_\infty = 0.908$ past a 6% thick circular arc airfoil of chord length $c = 1$ on a 51×51 mesh, with 21 equi-spaced points over the airfoil and stretched to far field boundaries 50 chord lengths away.

This exercise was also given in Section 6.4 using the Transonic Small Disturbance equation to describe the flow.

Solution Approach: We can, as before in Section 6.4, normalize pressure and density so that $p_\infty = 1$ and $\rho_\infty = 1$. We can use $\phi = V_\infty x$, with $V_\infty = M_\infty a_\infty$ and $a_\infty = \sqrt{\dfrac{\gamma p_\infty}{\rho_\infty}}$, as an initial condition. Because of the symmetry of the flow only the top or bottom half of the flow field needs to be calculated. We place the chord line of the airfoil along the lower boundary given by

$y = 0$ and the top, left and right far field boundaries 50 chord lengths away. The far field upstream and downstream boundary conditions are of Type (1). Along the far field boundaries ϕ is held constant and along the lower boundary the following boundary condition on the derivative of ϕ is used.

$$\left.\frac{\partial \phi}{\partial n}\right|_{body} = 0 \quad for \quad 0 \le x \le c \quad and \quad \frac{\partial \phi}{\partial y} = 0 \quad otherwise.$$

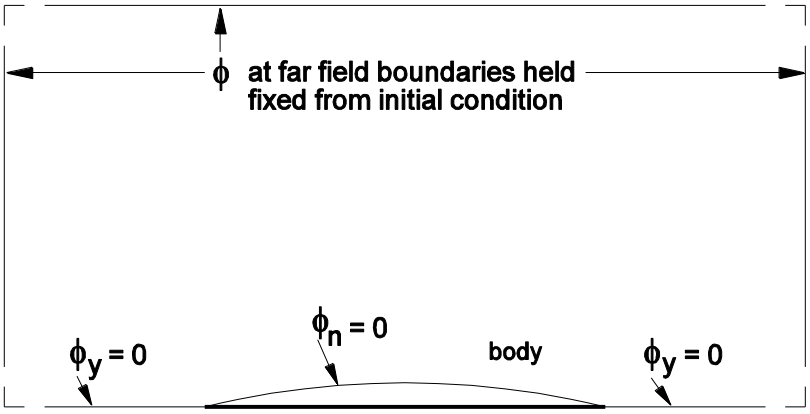

Figure 8.4 Flow volume about symmetric circular arc airfoil

A mesh similar to that shown in Section 6.4, but fitted along the body surface, is shown in the figure below. This mesh was formed by algebraically pushing up the mesh from Section 6.4 to account for the body thickness.

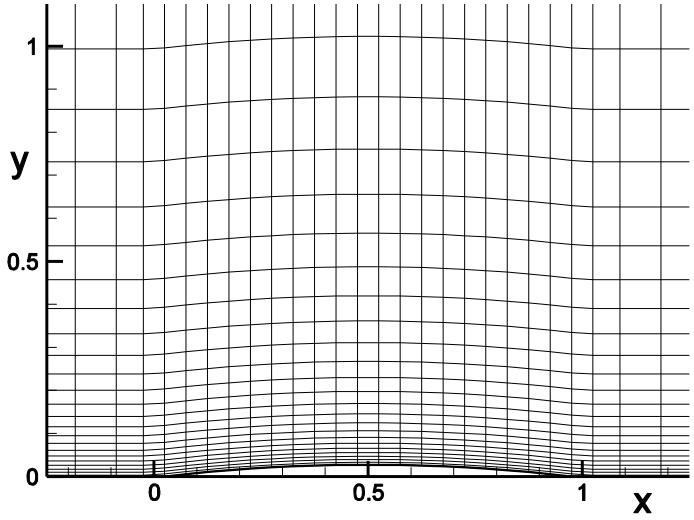

Figure 8.5 Mesh near airfoil.

The solutions to the Full Potential equation for both the subsonic and supersonic cases are shown in the following figures.

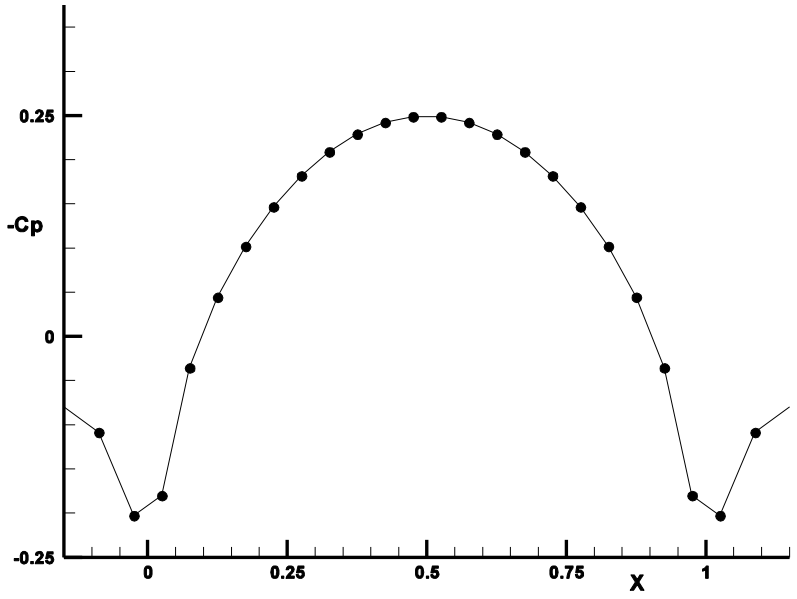

Figure 8.6 c_p vs. x for subsonic flow with $M_\infty = 0.735$

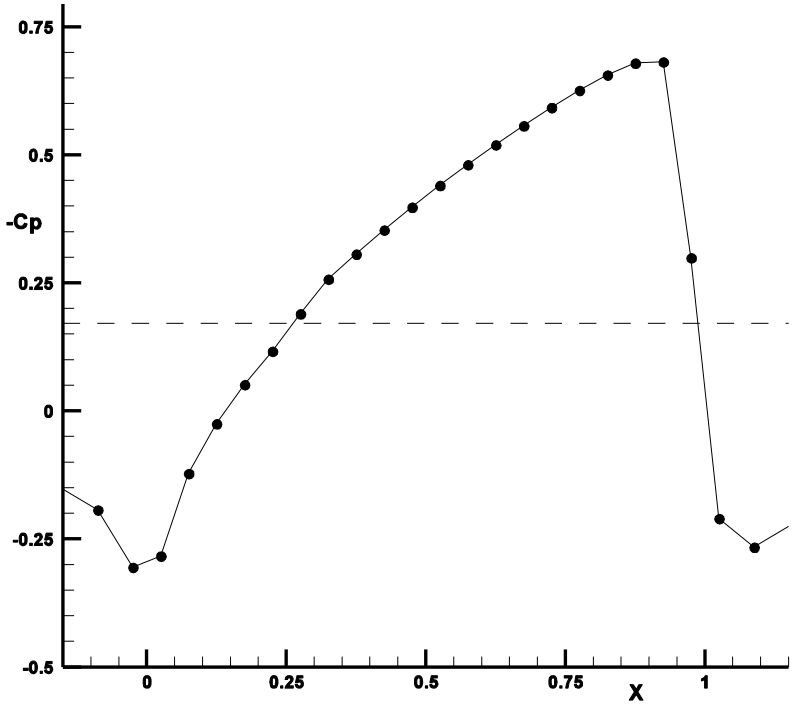

Figure 8.7 c_p vs. x for transonic flow with $M_\infty = 0.908$

The dashed line in Fig.8.7 represents c_p^*, the value of c_p when the local velocity equals the speed of sound. Values above this line indicate supersonic flow.

From Equation 8.2.2 $$(V^*)^2 = (a^*)^2 = a_\infty^2 \frac{1+\frac{\gamma-1}{2}M_\infty^2}{1-\frac{\gamma-1}{2}} = V_\infty^2 \frac{\frac{1}{M_\infty^2}+\frac{\gamma-1}{2}}{1-\frac{\gamma-1}{2}}$$

$$p^* = p_\infty \left[1-\frac{\gamma-1}{2}M_\infty^2\left(\frac{(V^*)^2}{V_\infty^2}-1\right)\right]^{\frac{\gamma}{\gamma-1}} \text{ and } c_p^* = \frac{p^*-p_\infty}{\frac{1}{2}\rho_\infty V_\infty^2}$$

The solutions to both the Transonic Small Disturbance and Full Potential equations on a 101×51 mesh are compared in the figure below.

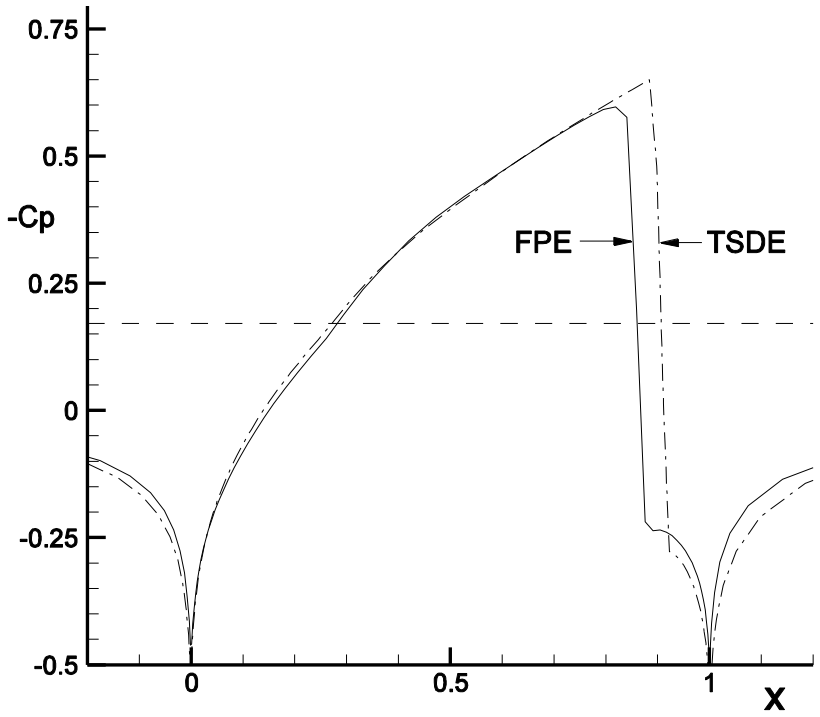

Figure 8.8 Comparison of c_p vs. x for transonic flow with $M_\infty = 0.908$ for both the Transonic Small Disturbance and Full Potential equations.

8.4.2 Applications 2 : Flow Past a Right Circular Cylinder

Exercise: Solve for Case (1) non-lifting flow and Case (2) lifting flow past a right circular cylinder at $M_\infty = 0.2$ on a 30×22 mesh, with 28 equi-spaced points wrapped about the cylinder and 20 stretched from the body surface to the far field boundary $50r$ away, with body radius $r = 0.5$.

Solution Approach: Again we normalize pressure and density so that $p_\infty = 1$ and $\rho_\infty = 1$. We again use $\phi = V_\infty x$, with $V_\infty = M_\infty a_\infty$ and $a_\infty = \sqrt{\frac{\gamma p_\infty}{\rho_\infty}}$, as an initial condition. A circular mesh about the cylinder and stretched, using the simple stretching function of

Section 5.3.1 with $\Delta r_{\min} = 0.04r$, is shown in the figure below. This type of grid is often referred to as an O-type mesh.

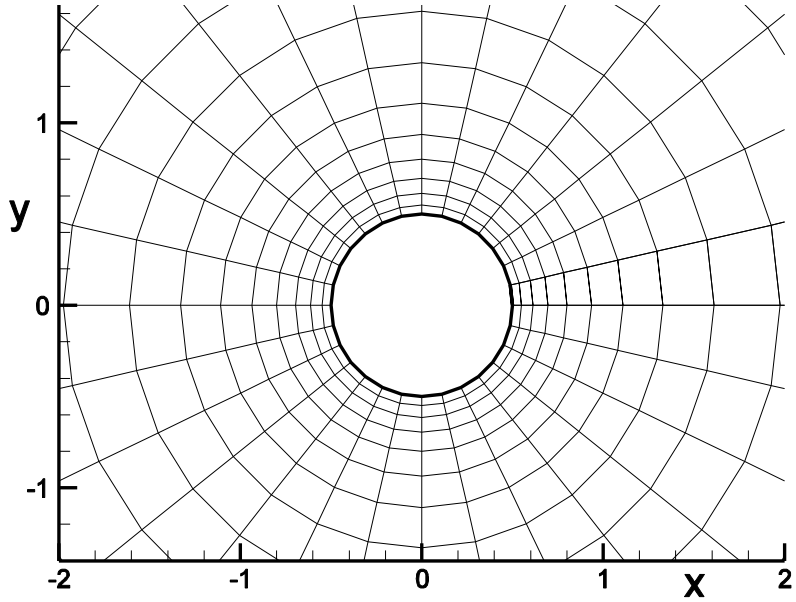

Figure 8.9 Mesh about circular cylinder**.**

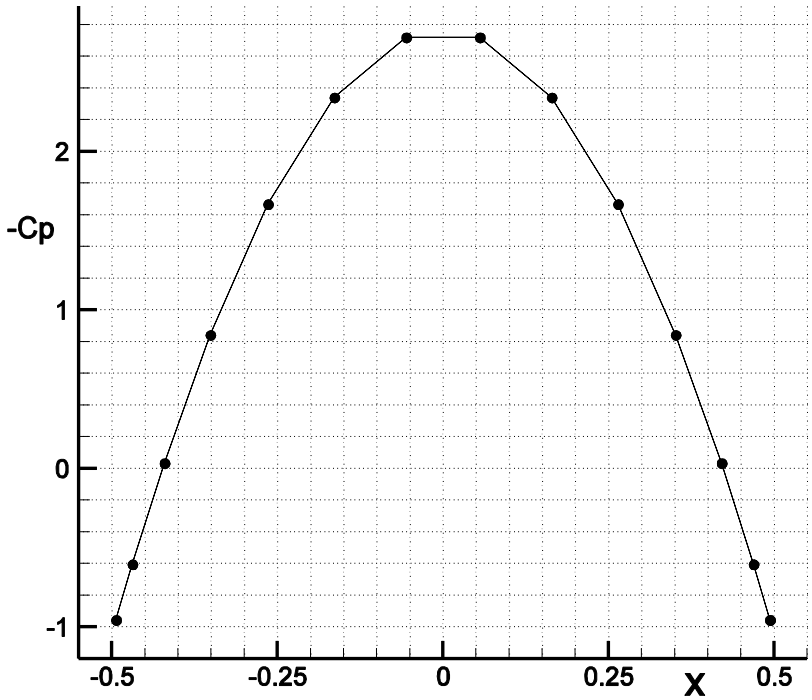

Figure 8.10 c_p vs. x for non-lifting flow about cylinder.

The pressure coefficient along the "chord" line, $-0.5 \le x \le 0.5$ and $y = 0$, is shown in the figure above for the non-lifting case. Because the flow is symmetric with respect to the chord line both the upper and lower surface pressure distributions are coincident with

zero net lift. The streamlines past the cylinder for this case are shown in the figure below. The flow is also symmetric with respect to the vertical line through the origin, which results in zero drag.

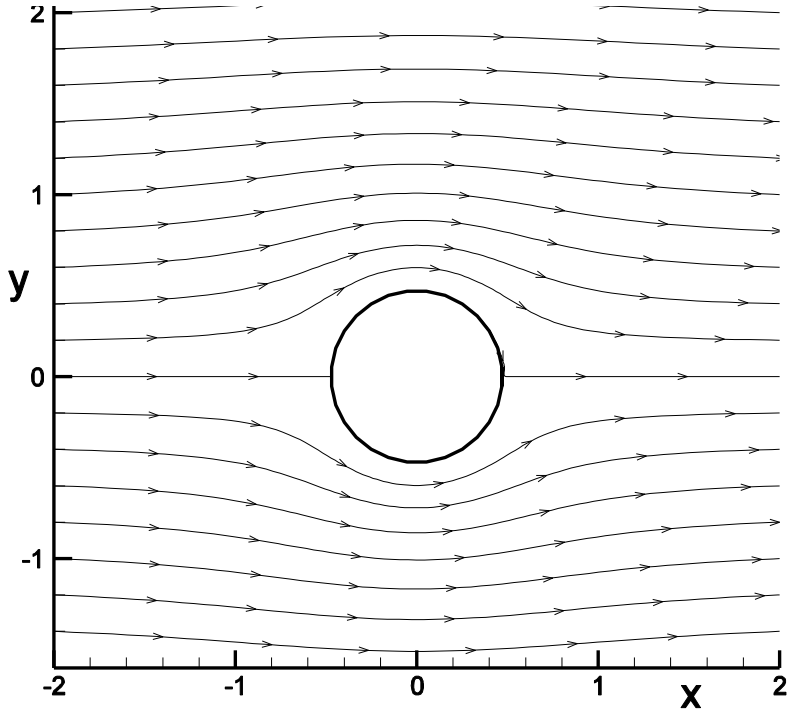

Figure 8.11 Streamlines about cylinder for no-lift.

For the lifting case a vortex should be added to the initial condition for determining ϕ and must also be included along the outer boundary of the flow field (See Anderson, **Fundamentals of Aerodynamics**, McGraw-Hill).

$$\phi = V_\infty x - \frac{\Gamma}{2\pi}\theta$$

The circulation is given by $\Gamma = -\oint_C \vec{V}\cdot d\vec{l}$ about any contour C and θ is measured from the positive x-axis in the counter clockwise direction. The value for circulation used for the lifting Case (2) is $\Gamma = 3.29$. As θ increases along a contour about the body (counter clockwise direction), ϕ decreases. From $0 \to 2\pi$ ϕ decreases by one Γ. Therefore there is a discontinuity in ϕ as the solution at $\theta = 2\pi$ meets the solution at $\theta = 0$, located at the same point in space. The Type (2) boundary condition needs to be modified for lifting flows as follows.

$$\phi_{I,j} = \phi_{2,j} + \Gamma \text{ and } \phi_{1,j} = \phi_{I-1,j} - \Gamma$$

The pressure coefficient along the cylinder surface, over $-0.5 \le x \le 0.5$, is shown in the figure below for the lifting case. This flow is asymmetric with respect to the chord line

and both the upper and lower surface pressure distributions are distinct. The streamlines past the cylinder for this case are shown in the figure below. The flow is, however, still symmetric with respect to the vertical line through the origin, which results in zero drag.

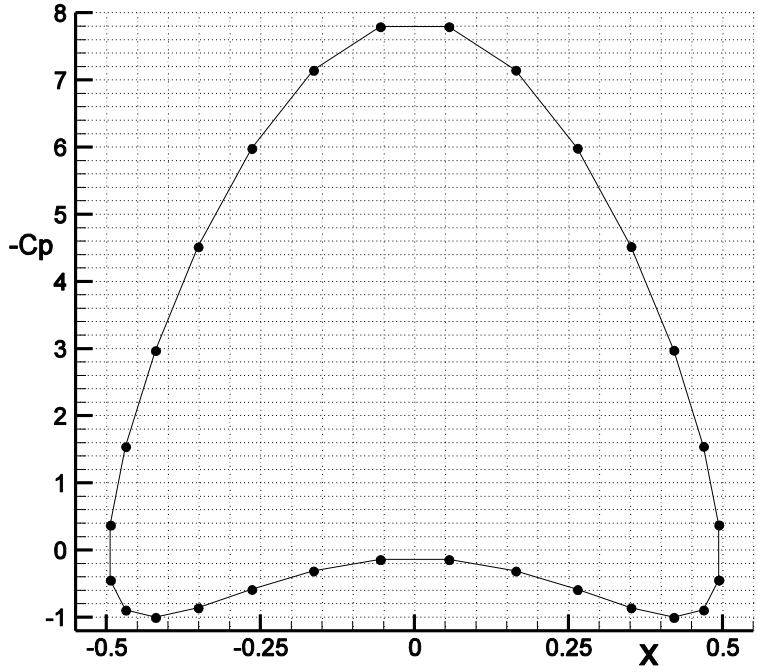

Figure 8.12 c_p vs. x for lifting flow about cylinder.

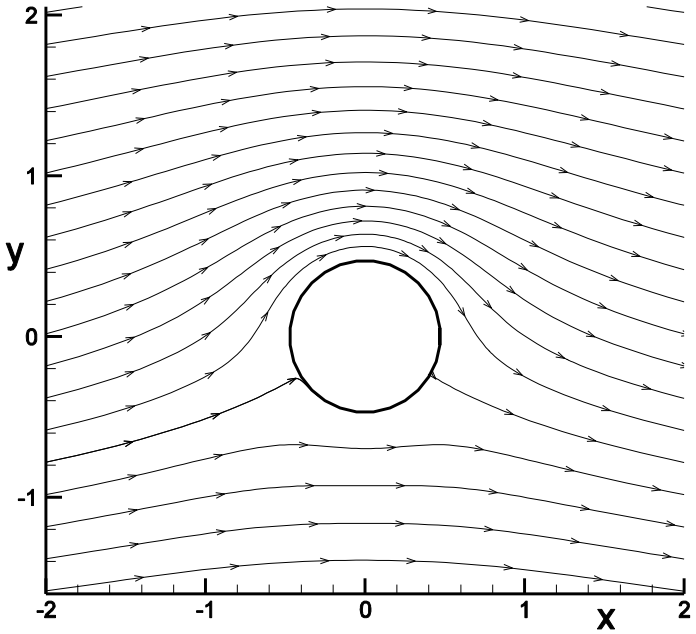

Figure 8.13 Streamlines about a lifting cylinder.

8.4.3 Applications 3 : Flow Past an Ellipse

Exercise: Solve for $M_\infty = 0.2$ flow past a $6-1$ ellipse at 5^o angle of attack on a 60×44 mesh, with 58 non-equi-spaced points wrapped about the ellipse and 42 stretched from the body surface to the far field boundary at least 25 body thicknesses away.

Solution Approach: Again we normalize pressure and density so that $p_\infty = 1$ and $\rho_\infty = 1$. We now set $\phi = V_\infty\left(x\cos\alpha + y\sin\alpha\right)$, with $\alpha = 5^o$, $V_\infty = M_\infty a_\infty$ and $a_\infty = \sqrt{\dfrac{\gamma p_\infty}{\rho_\infty}}$, as an initial condition. The circulation Γ has been set to zero. Again we wrap a mesh about the complete body. The O-type mesh about the ellipse is shown in the figure below.

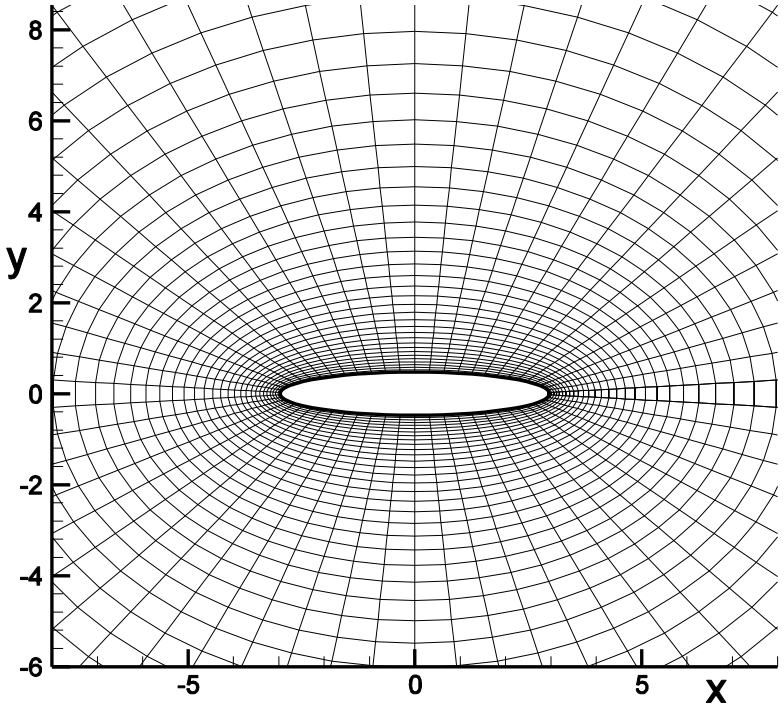

Figure 8.14 O-type mesh about a $6-1$ ellipse**.**

This mesh was first constructed for a right circular cylinder, with 58 equi-spaced points wrapped about the cylinder. Then the mesh was stretched in the x-direction by $x \leftarrow 6x$ for the $6-1$ ellipse.

Because no circulation has been introduced into the flow no lift should occur even though the body is at 5^o angle of attack. The streamlines about the ellipse and the pressure coefficient distribution are shown in the figures below. The streamline symmetry above and below and fore and aft indicate no lift and no drag, respectively. The symmetric c_p distribution confirms the zero lift observation.

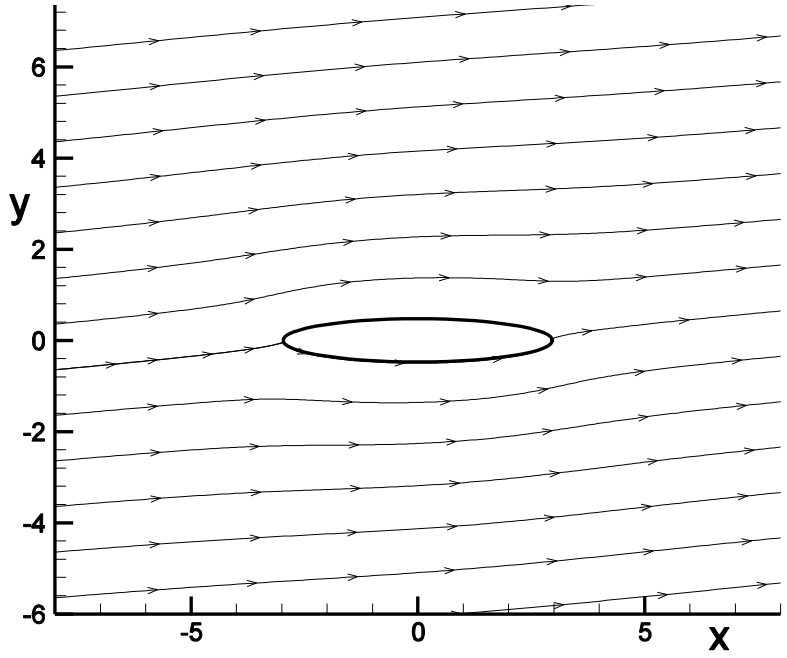

Figure 8.15 Streamlines about ellipse.

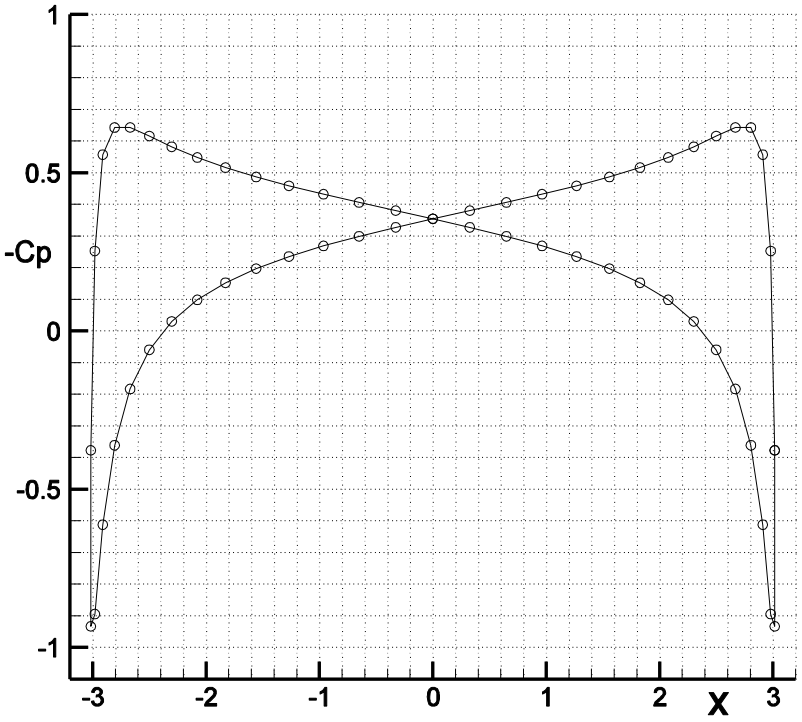

Figure 8.16 c_p vs. x for flow about an ellipse.

8.4.4 Applications 4 : Flow Past an NACA0012 Airfoil

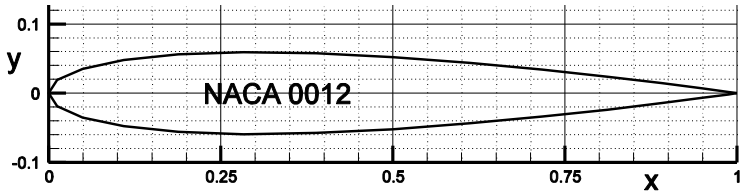

Figure 8.17 NACA0012 airfoil

Exercise: Solve for $M_\infty = 0.75$ flow past an NACA0012 airfoil of chord length $c = 1$ for Case (1) 0^o angle of attack and Case (2) at 1^o angle of attack, on a 30×22 mesh, with 28 non-equi-spaced points wrapped about the airfoil and 20 stretched from the body surface to the far field boundary at 50 chord lengths away.

Solution Approach: Again we normalize pressure and density so that $p_\infty = 1$ and $\rho_\infty = 1$. We now set $\phi = V_\infty \left(x\cos\alpha + y\sin\alpha \right) - \dfrac{\Gamma}{2\pi}\theta$, with angle of attack α, $V_\infty = M_\infty a_\infty$ and $a_\infty = \sqrt{\dfrac{\gamma p_\infty}{\rho_\infty}}$, as an initial condition. For Case (2) the circulation Γ is not known before hand. Again, a mesh is wrapped about the complete body to implement the Type (2) boundary conditions. The O-type mesh about the airfoil is shown in the figure below.

NACA0012 Coordinates	
x	y
1.00000E+00	-8.86156E-09
9.87464E-01	-1.76456E-03
9.50484E-01	-6.81334E-03
8.90916E-01	-1.44879E-02
8.11745E-01	-2.38897E-02
7.16942E-01	-3.40255E-02
6.11260E-01	-4.38446E-02
5.00000E-01	-5.21902E-02
3.88740E-01	-5.77928E-02
2.83058E-01	-5.94367E-02
1.88255E-01	-5.62520E-02
1.09084E-01	-4.80096E-02
4.95155E-02	-3.52132E-02
1.25361E-02	-1.88663E-02
3.95762E-09	8.90630E-08
1.25361E-02	1.88663E-02
4.95156E-02	3.52132E-02
1.09084E-01	4.80096E-02
1.88255E-01	5.62520E-02
2.83058E-01	5.94367E-02
3.88739E-01	5.77928E-02
5.00000E-01	5.21902E-02
6.11261E-01	4.38445E-02
7.16942E-01	3.40255E-02
8.11745E-01	2.38897E-02
8.90916E-01	1.44879E-02
9.50484E-01	6.81334E-03
9.87464E-01	1.76456E-03
1.00000E+00	-8.86156E-09

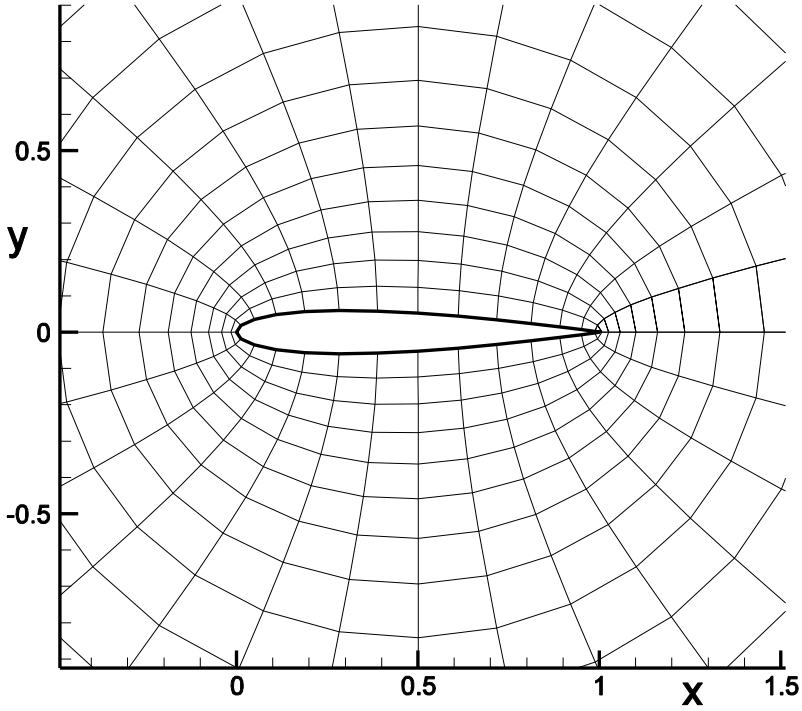

Figure 8.18 Mesh about an NACA0012 airfoil**.**

For Case (1) $\Gamma = 0$ and the flow above and below the airfoil is symmetric. Therefore the upper and lower surface pressure coefficient distributions are equal as shown in the figure below. Some supersonic flow is indicated by the "dashed line" location of c_p^* in the figure.

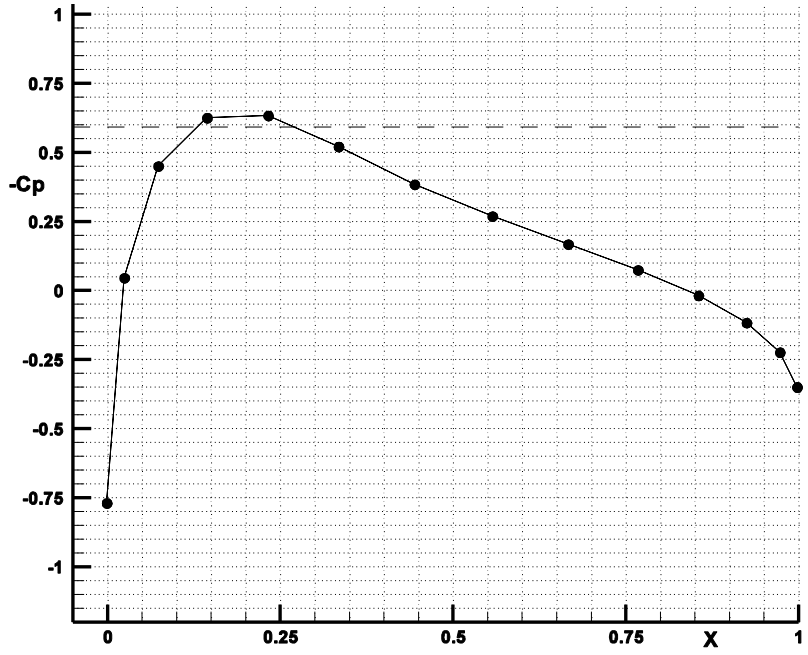

Figure 8.19 c_p vs. x for flow Case(1).

For Case (2) the angle of attack causes the flow above and below the airfoil to be different as shown in the figure below, for which the circulation has been set to $\Gamma = 0$. Of course, this numerical experiment is not compatible with airfoils at an angle of attack that produce lift. The NACA0012 airfoil is symmetric and should produce lift and circulation at any nonzero angle of attack. The incompatibility is shown in the figure by the jump in pressure at the trailing edge of the airfoil, a violation of the Kutta condition. However, the solution of the Full Potential equation about even sharp trailing edge airfoils will yield this non-physical solution. Integration of pressure about the airfoil for this solution will yield a value for the lift coefficient $c_l = -0.0006$, essentially zero for the numerical accuracy of this coarse mesh calculation. This remarkable result indicates the power of circulation to determine lift (the Kutta-Joukowski Theorem).

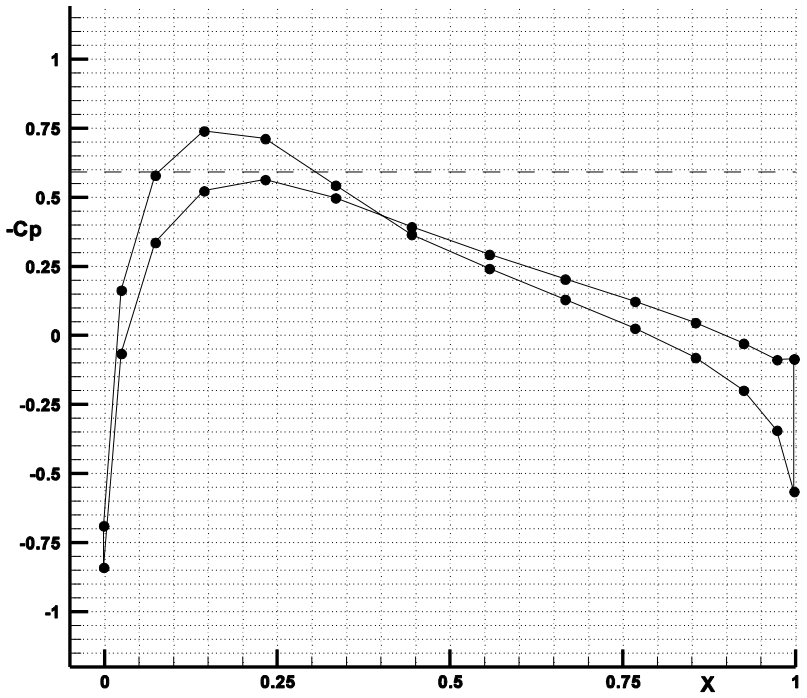

Figure 8.20 c_p vs. x for flow Case(2) with $\Gamma = 0$.

The question now is how to determine the circulation Γ such that the Kutta Condition is satisfied. A good start would be to use thin airfoil theory, with the Prandtl-Glauert compressibility correction factor, followed by the Kutta-Joukowski Theorem to set Γ initially.

$$c_l = 2\pi\alpha, \quad c_l \leftarrow \frac{c_l}{\sqrt{1-M_\infty^2}}, \quad L' = c_l \tfrac{1}{2}\rho_\infty V_\infty^2 c \quad \textit{and} \quad \Gamma = \frac{L'}{\rho_\infty V} \qquad (8.3.1)$$

Then, during the solution for ϕ, the circulation is set again at the end of each iteration step by the difference in ϕ at the trailing edge, $\Gamma = \phi_{IL-1,2} - \phi_{2,2}$, (see figure below).

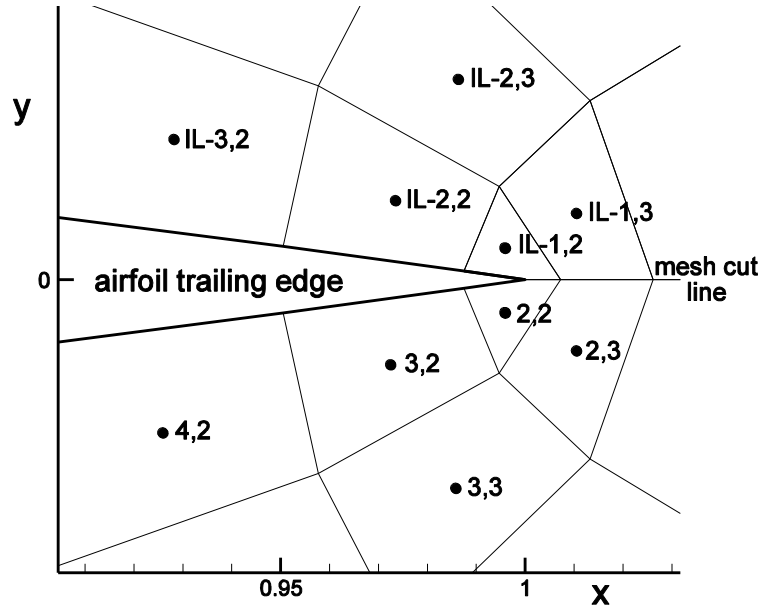

Figure 8.21 Mesh at trailing edge of airfoil.

The calculation was repeated with Γ allowed to adjust according to the equation $\Gamma = \phi_{IL-1,2} - \phi_{2,2}$ and the pressure coefficient distribution is shown in the figure below.

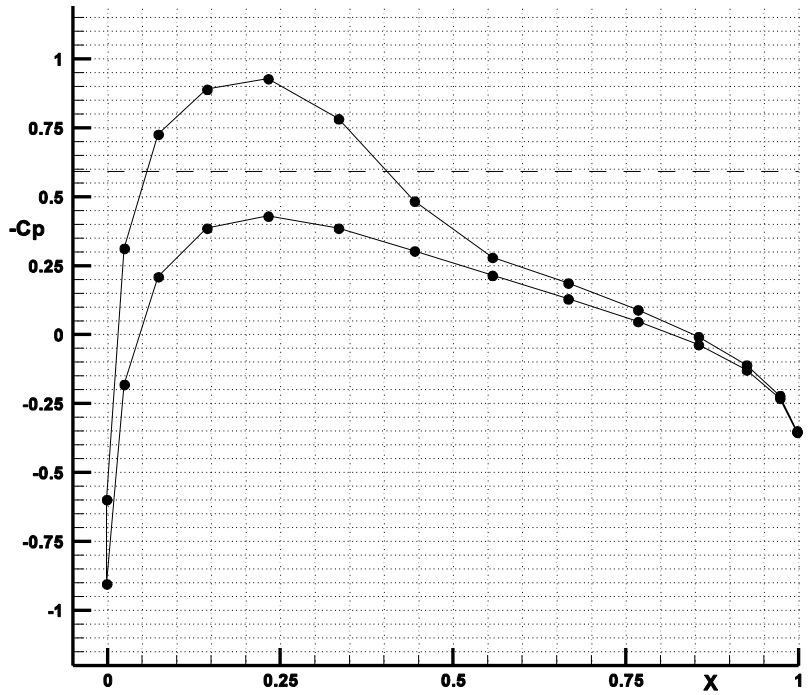

Figure 8.22 c_p vs. x for flow Case(2), $c_l = 0.23$.

The steep pressure gradient crossing through the c_p^* dashed line at the end of the supersonic region indicates the presence of a shock wave, which is not well defined on this coarse mesh. This case was recalculated on finer meshes. The results, shown in the figures below, clearly show the improvement in shock wave capturing with finer meshes.

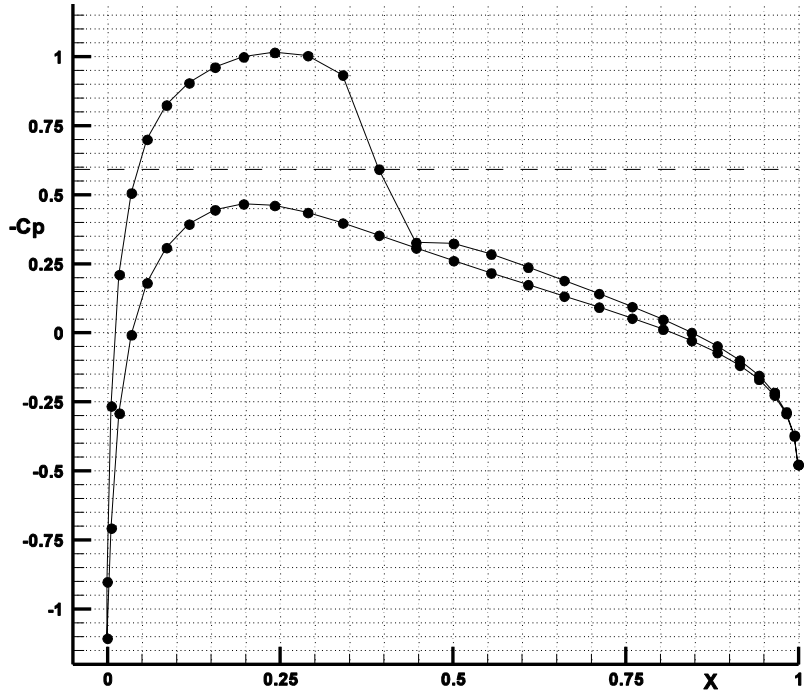

Figure 8.23 c_p vs. x on a 60×38 mesh, $c_l = 0.23$

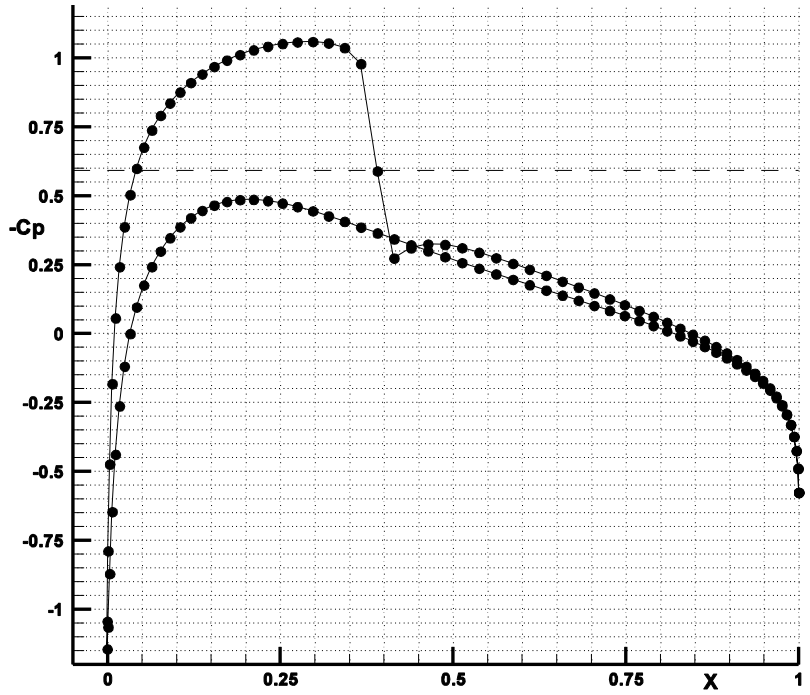

Figure 8.24 c_p vs. x on a 130×82 mesh, $c_l = 0.23$.

Mach contours and streamlines about the NACA0012 airfoil foil in $M_\infty = 0.75$ flow at 1^o degree angle of attack are shown below.

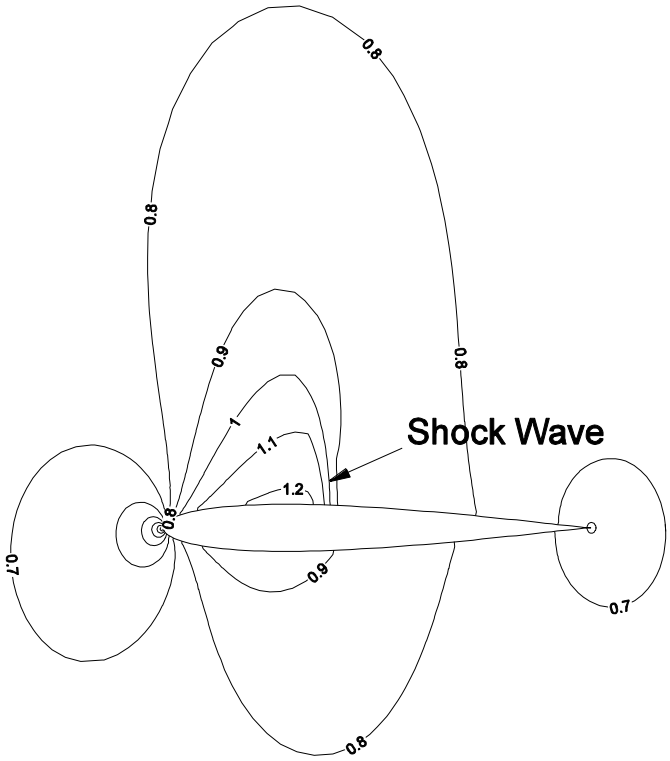

Figure 8.25 Mach contours

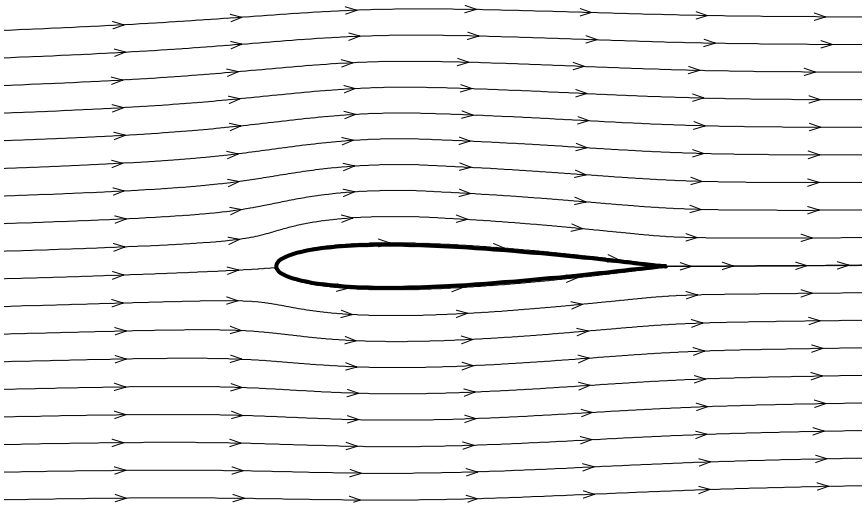

Figure 8.26 Streamlines